Dehydration of Oxide:Water Interfaces by Brines Quantified with Nonlinear Spectroscopy

Nicole M. Gonzalez,[§] Amani O. Alghamdi,[§] and Franz M. Geiger[*]

Department of Chemistry, Northwestern University

2145 Sheridan Road, Evanston, IL 60202, USA

Abstract. Counting the number density of ions and water molecules at aqueous:solid interfaces remains a fundamental challenge, especially under conditions of varying ionic strength. Here, we employ an all-optical non-contact approach based on phase- and amplitude-resolved second harmonic generation spectroscopy to estimate the cation and anion coverages and the number density of net-aligned water molecules at fused silica surfaces in contact with aqueous solutions held at pH 5.8 and a wide range of ionic strengths of NaCl, $NaClO_4$, Na_2SO_4, and Na_2HPO_4 up to 8 M. At 8 M ionic strength of $NaClO_4$, the data are consistent with an interface that is comprised of half of a monolayer of ions ($\theta_{Na^+} + \theta_{ClO_4^-} \approx 5 \times 10^{14}$ cm^2) and half of a monolayer of water molecules ($\theta_{H_2O} \approx 4 \times 10^{14}$ cm^{-2}), the latter having flipped their dipolar orientation from "protons to the surface" to "oxygens to the surface". The interfacial water:total ion ratio is close to ten times smaller than in the bulk solution at these high ionic strengths. The Helmholtz free energy associated with water disordering increases abruptly from near 0 kJ mol^{-1} below 2 M ionic strength to 10 kJ mol^{-1} at 8 M ionic strength, indicating perhaps a Kirkwood-like transition from a hydrated to a dehydrated interface.

[§]Authors contributed equally to this work

*Corresponding author: f-geiger@northwestern.edu

Introduction. Highly concentrated electrolytes are ubiquitous in both natural and engineered systems, spanning a wide range of environments from confined biological zones like synaptic clefts (~0.1-0.15 M)[1] to geochemical oil reservoirs (~6 M)[2] and oceans (~0.6 M).[3,4] They play essential roles in advanced technologies, including electrocatalysis,[5] batteries (~0.5-1.5 M),[6,7] supercapacitors (1-2 M),[8] drug delivery,[9] and saline aquifers proposed for carbon dioxide sequestration (< 2 M).[10] Despite their prevalence, a comprehensive molecular-level understanding of their behavior, particularly at charged surfaces, remains elusive.[11,12] Beyond 1 M ionic strength, the decay screening length at solid:aqueous interfaces has been reported to lengthen as opposed to shortening, an observation that is at variance with Debye-Hückel theory.[13-20] Similar findings have been reported for aqueous bulk solutions.[21,22] Despite the surge in publications in this area,[23-27] many relying on scanning probes,[15,16,28-31] the number density of interfacial water molecules, cations, and anions have not yet been quantified experimentally as a function of ionic strength, the focus of this present study.

Excluded volume, dielectric saturation, ion-ion correlations, and hydration structure are considered key factors for explaining anomalous underscreening on various solid surfaces.[13] Most studies involving scanning probes attribute the similarity in force profiles between ionic liquids and highly concentrated 1:1 electrolytes to electrostatic origins. These studies conjecture that strong ion-ion correlations form correlated ionic clusters in which the few remaining free water molecules are not isolated but integrated into the cluster.[16,32] Despite structural and compositional differences, ionic liquids and concentrated electrolytes exhibit similar screening behavior when analyzed in terms of Bjerrum length, the diameter of the ions, and their activity coefficients.[32] Additional scanning probe studies that distinguish hydration structures and hydrated-ion correlations show that the apparent size of hydrated ions decreases as concentration increases.[31] At concentrations above 100 mM, the data are consistent with the formation of a 1-3 nm thick

ionic solid at the surface, suggesting a water-ion coordination number of less than one.[31] Despite the valuable insights these studies offer, it remains challenging to quantify the number of water molecules, cations, and anions at the Stern layer in such measurements.

Advanced theoretical models that extend beyond the classical Debye-Hückel framework have significantly deepened our understanding of electrolyte behavior. While these approaches neglect the role of charged surfaces, they offer critical insights into finite ion size effects and ion-ion correlations through the lens of statistical mechanics. For example, Kirkwood and Poirier[33] developed a correlation function that decays with damped oscillation rather than the typical Yukawa exponential decay commonly employed when using Debye-Hückel theory. Kirkwood transitions were recently reported using small-angle X-ray experiments[34] and incorporated into simplified mean-field theory models with a modified Coulomb interaction to account for finite ion size, allowing for an analytical derivation of the anomalous screening length from the charge-charge correlation function.[35] Kirkwood and Poirier's statistical treatment was also revisited by Kjellander to incorporate nonlocal electrostatics between the ions in the description of Debye-Hückel's theory and the description of the permittivity.[36] The aforementioned theory, referred to as dressed ion-molecule theory, seems to infer that ionic structuring and correlation-driven layering arise in highly concentrated electrolytes.

Our investigation aims to understand how water and ions arrange themselves on a charged solid surface at high ionic strength. We ask how many interfacial anions, cations, and water molecules are present at a given salt concentration, how the ratio of ion pairs to water molecules varies with ionic strength, and how the Helmholtz free energy of interfacial water molecules changes with increasing ionic strength to brine-like conditions. We describe an experiment that estimates water, anion, and cation coverage on a fused silica surface over a wide range of ion concentrations. While X-ray-based techniques can provide exquisite structural information

regarding ions at such high concentrations,[37] they are currently limited to atomically flat substrates like mica and high-Z elements. Vibrational spectroscopy yields OH stretching spectra of interfacial water molecules at high concentrations on silica surfaces.[38] However, quantitative methods to count interfacial water molecules, cations, and anions are just beginning to emerge.[39-41] In this work, we employ non-resonant phase- and amplitude-resolved second harmonic generation (SHG) spectroscopy to determine the interfacial second-order susceptibility ($\chi^{(2)}$) and the total interfacial potential ($\Phi(0)_{tot}$), from which we estimate the coverage of anions, cations, and net-aligned water molecules within the Stern layer. Our findings are consistent with interfacial dehydration, resulting in a water:total ion ratio approaching unity at 8 M $NaClO_4$. The abrupt change in the Helmholtz free energy associated with water reordering is perhaps of a Kirkwood transition in which the interface dehydrates at ionic strengths exceeding ~2 M.

Experimental Methods. In the experiments, we used 1 mm thin fused silica windows ($\lambda/10$) from Edmund Optics (11876) cleaned as described in our earlier work.[40] We employed a flow rate of 10 mL min^{-1}. The experiments were carried out in at least duplicate on four different substrates, each time starting with water from a MilliQ system that had been left to equilibrate with laboratory air overnight (so ambient carbonate is present in the solutions). We employ a Ytterbium crystal-based oscillator driving a phase- and amplitude-resolved SHG spectrometer for tracking the interference between the sample SHG signal and a local oscillator produced by a 50 μm thin quartz wafer moving relative to the sample, as recently described.[40] Each fringe took 75 seconds to complete, including the time to reset the translational stage for the next scan. The experiments were carried out using NaCl, $NaClO_4$, Na_2SO_4, and Na_2HPO_4, to cover mono- and divalent anions in the Hofmeister series and to access up to 8 M ionic strength in the case of $NaClO_4$. Details regarding solution preparation can be found in the Supporting Information. Briefly, the aqueous solutions are prepared by placing a known mass of a given salt into a volumetric flask and then filling the

volumetric flask with water from a MilliQ system to the 1 L mark. By means of example, placing 292 g of NaCl into the volumetric flask and adding water up to the 1 L mark produces a 5 M, or 5.63 m, solution. For the highest concentration we used (8M, or ~13.3 m, $NaClO_4$), the water-to-total ion ratio on a per mol basis is ~3.5, while the water-to-mean ion activity ratio is ~0.05 (here, we used the classic compilation by Hamer and Wu).[42] Higher ionic strengths required considerable time for the SHG amplitude and phase to reach steady state, typically on the order of an hour or more with each new concentration (please see Supporting Information Figures S1 and S2). The highly stable output of our Light Conversion Flint oscillator makes these measurements possible.

Results and Discussion. Fig. 1A shows SHG interference fringes recorded as a function of the position of the LO source for each of the $NaClO_4$ concentrations we studied (each mm difference in stage position corresponds to 3.158° in the SHG phase).[43,44] As in our prior studies, the SHG amplitude first increases and then decreases (Fig. 1B) with increasing ionic strength[45] while the phase delays (Fig. 1C) over this ionic strength range. Both values are obtained from a sine fit. The amplitude is normalized to deionized water, and the phase is referenced to the one obtained at the point of zero charge (1 M $NaClO_4$ at pH 2.5). With increasing ionic strength, the phase shifts by 60-80° while the amplitude decreases by > 90%. We then employ an optical model[40,43,46,47] connecting the SHG amplitude and phase responses from fused silica:aqueous interfaces to the properties we seek, namely the second-order nonlinear susceptibility, $\chi^{(2)}$, and the total potential $\Phi(0)_{tot}$. The first yields, to leading order, the number of net-aligned water molecules in the Stern layer, while the latter is used further below to compute an estimate for the ion coverages. The latter is the sum of electrostatic potential contributions from the mobile charges (those that are captured in Gouy-Chapman-Stern theory as - and + charges of, say, chloride and sodium ions) and the bound charges (say, the 18 electrons on a water molecule).

We use a wave vector mismatch in the model of Δk_z=2.5 × 10^7 m^{-1}in our spectrometer for $\omega = 1030\ nm$ and $2\omega = 515\ nm$ as the ionic strength-dependent variations in the refractive index as outlined in the Supporting Information Section S3 are negligible. Modifying the decay length λ_D in the DC phase angle expression in our model (φ_{DC}=arctan($\Delta k_z \lambda_D$), where λ_D is the Debye length)[43,44,48-50] to match values reported in anomalous underscreening studies[16] does not alter the results presented here, given the magnitude of Δk_z (please see Supporting Information Fig. S4).

From Second-Order Nonlinear Susceptibility to Number of Net-Aligned Water Molecules per cm². As shown in Fig. 2A, the second-order nonlinear susceptibility ($\chi^{(2)}$) is positive across the entire ionic strength range surveyed but decreases as the ionic strength increases, indicating a gradual loss of net interfacial order. We find that the more polarizable ions are associated with a somewhat larger second-order nonlinear susceptibility. At aqueous interfaces, a positive $\chi^{(2)}$ value generally reflects water dipoles oriented with their negative ends pointing into the bulk (H away from water), as established by second harmonic scattering,[51,52] phase-resolved SFG experiments[53] (most readily demonstrated by the positive $\chi^{(2)}$ value of the dangling free OH stretch of the air:water interface),[54] and variable-angle surface spectroscopy.[55] Therefore, we conclude that the observed positive $\chi^{(2)}$ indicates a net orientation in which interfacial species contributing to $\chi^{(2)}$ are aligned with their negative ends pointing into the water. These contributors include, in order of abundance, Stern layer water molecules, surface SiOH, SiO^-, and $SiOH_2^+$ groups, as well as specifically and non-specifically adsorbed ions and ion pairs of Na^+ and ClO_4^-.[50,56] As the ions studied here are centrosymmetric, their nonlinear hyperpolarizabilities should be small or even zero when compared to water, at least to leading order. In other words, we assume that $\chi^{(2)} = \mathcal{N} < \alpha^{(2)} >$ is dominated by the orientational average of the water molecules' molecular hyperpolarizability, consistent with previous SFG studies.[56] Yet, we note that electronic structure calculations of aqueous ions' hyperpolarizabilities are currently lacking. As we reported

earlier,[41,47,57] $\chi^{(2)}$ yields the number of net-aligned Stern layer water molecules, $\mathcal{N}_{\uparrow}$, according to Eq. 1:

$$\mathcal{N}_{\uparrow} = \frac{\left[\chi^{(2)} - \chi^{(2)}_{\mathrm{SiO_2,\ point\ of\ zero\ charge}}\right]\varepsilon_r\varepsilon_0}{\alpha^{(2)} \cdot 10^4 \mathrm{cm^2 m^{-2}}} \qquad (1)$$

Provided that $\chi^{(2)}$ is dominated by the net alignment of Stern layer water, we can remove the silica-only contribution, which we obtain, to leading order, at the point of zero charge ($\chi^{(2)}_{\mathrm{SiO_2,\ point\ of\ zero\ charge}} = 1.7 \times 10^{-22}$ $\mathrm{m^2V^{-1}}$ as measured in our experiment using 1 M NaCl at pH 2.5).[43] We employ an interfacial relative permittivity of water's static refractive index squared ($\varepsilon_r = 1.8$),[41] the vacuum permittivity (ε_0), and an MP4-derived molecular hyperpolarizability estimate of a water molecule in a liquid water model of $\alpha^{(2)} = 4.2 \times 10^{-52}$ $\mathrm{Cm^3V^{-2}}$ (this value is the $\alpha^{(2)}_{xxz} = \alpha^{(2)}_{xzx}$ tensor element estimate to which our s-in/p-out polarization combination is sensitive).[57-59] Accessing other polarization combinations to probe water molecules oriented parallel to the interface is currently not possible in our setup given the polarization of the fundamental and the second harmonic in our calcite time delay compensator. We emphasize that these values are estimates as the Stern layer water density has not yet been determined experimentally for silica:water interfaces at these brine conditions. Atomistic simulations indicate it to be subject to more than two-fold z-dependent undulations for the first few Å.[60,61] Moreover, the values are upper bounds as the Stern layer water molecules are likely not subject to a purely up or down distribution but instead to a multimodal orientation distribution (including various tilt angles) that is currently unknown.

Fig. 2B shows that up to 10 mM $NaClO_4$ ionic strength, our estimate of the net-aligned Stern layer water molecules remains largely constant. A monolayer of water molecules on ice or liquid water corresponds to ~1.1 x 10^{15} cm^{-2}, given the density of water or ice, so eqn. 1 results in a few monolayers of net-aligned Stern layer water molecules having their H↠O dipoles pointing

away from the interface. As the ionic strength increases, the number of water molecules net-aligned that way decreases, which is consistent with previous SFG observations that indicate water structure disruption with increasing ionic strength on the surface of silica.[38,62,63] At 5 M $NaClO_4$, the number of water molecules having their H↠O dipoles pointing away from the interface crosses through zero (Fig. 2B inset), indicating an equal number of water molecules having their H↠O dipoles pointing away from and towards the interface. At higher ionic strengths, the second-order non-linear susceptibility difference relative to its PZC value becomes negative, so the number of net-aligned water molecules becomes negative. This result indicates the presence of a small excess of Stern layer water molecules having their H↠O dipoles pointing towards the surface. Next, we address the ion coverages, which we obtain from the interfacial potential.

From Total Interfacial Potential to Number of Cations and Anions per cm². Fig. 2C shows that the total interfacial potential increases monotonically with increasing ionic strength. Slight charge inversion may occur at > 5 M, similar to overcharging observed in recent X-ray reflectivity reports.[37] As stated above, the total interfacial potential contains the contributions from the bound and the mobile charges, the former being, for instance, the 18 electrons on a water molecule, the latter being the single positive or negative charge on a cation or an anion.[40] To assess the contribution from the ions, we attenuate the measured total potential by 90% as that factor accounts for the difference between the measured total and the Gouy-Chapman (ions only) potential at high ionic strength.[39] This attenuated electrostatic potential then yields the ion surface coverage estimates,[64] in units of cm^{-2}, according to[39,40,65]

$$[ion]_s = \left[\frac{[ion]_{bulk} \cdot N_A}{1000\ cm^3 dm^{-3}}\right]^{2/3} \cdot \left[e^{-[0.1 \cdot q_i \cdot \Phi_{tot} \cdot F](RT)^{-1}}\right] \qquad (2).$$

Here, $[ion]_{bulk}$ is the bulk ion concentration, N_A is Avogadro's number, q_i is the ion valency (+1 for Na^+, -1 for Cl^- and ClO_4^-, and -2 for HPO_4^{2-} and SO_4^{2-}), F is Faraday's constant, and RT is the thermal energy. For the high ionic strengths employed here, we also used the mean ion activities

of NaCl, $NaClO_4$, and Na_2SO_4[42,66-68] and experimentally determined single ion activities[69,70] for Na_2SO_4.[71] Varying the activity coefficients by a factor as large as ±2 translates into surface coverages that are $(\pm 2)^{2/3}$=[1.6, 0.6], or 60% and 40%, larger and smaller, respectively. Attenuating the total potential not by 90% but by 80% or 95% changes the ion coverage estimates from eqn. 2 by <10% at the higher ionic strengths, and about a factor of 2 at low ionic strength. In other words, the cation and anion surface coverage estimates are conservatively reliable to within a factor of about 2.

Water Orientation Flips at High Ionic Strength. Fig. 2D shows that cation coverage estimates exceed the anion coverages slightly, as would be expected for the negative surface potentials at this pH, even at high ionic strength. At 8 M $NaClO_4$, the cation and anion coverages are ~2.5 x 10^{14} cm^{-2} each. As the cation coverage is generally somewhat larger than the anion coverage, doubling it yields estimates for the ion pair coverage. The ion pairs, if they indeed form, could be solvent-separated or in the form of contact ion pairs, which our earlier atomistic simulations indicated to yield second-order nonlinear susceptibilities that recapitulate values from phase-resolved SHG experiments carried out at 100 mM ionic strength with a preference for contact ion pair formation.[72] At 8 M ionic strength of $NaClO_4$, our data are consistent with a total ion surface coverage of ~5 x 10^{14} cm^{-2} (this is the sum of Na^+ and ClO_4^- ions per cm^2). This surface coverage is about half of the total ion surface coverage (again, the sum of Na^+ and ClO_4^- ions per cm^2) on solid $NaClO_4$ computed from $NaClO_4$'s bulk density and molar mass (~1 x 10^{15} cm^{-2}). The number of net-aligned water molecules at this ionic strength is 4 x 10^{14} cm^{-2} (Fig. 2B), or about one half a monolayer of water having their dipolar orientation flipped from "protons to the surface" to "oxygen to the surface", as indicated by the sign change in $\Delta\chi^{(2)} = \chi^{(2)} - \chi^{(2)}_{SiO_2,\ \text{point of zero charge}}$. We caution that this result is based on a reliable estimation of the $\chi^{(2)}_{SiO_2,\ \text{point of zero charge}}$.

Interface Dehydration at High Ionic Strength and Associated Work. Fig. 2E shows that the interfacial water:total ion ratio thus dips below one at ~4 M ionic strength, reaching as low as 0.2 at 8 M $NaClO_4$, ten times lower than the water:total ion ratio in the bulk of an 8M (or 13.3 m) $NaClO_4$ solution on a per mol basis (2.1). This result is consistent with a dehydrated interface when compared to the bulk liquid at 8 M $NaClO_4$. The sum of the net-aligned water molecules and the Na^+:ClO_4^- ion pairs are ~8 x 10^{14} cm^{-2}, or close to a monolayer. The results indicate that net-aligned water is being replaced by incoming Na^+:ClO_4^- ions. Whether the ions and the water molecules are mixed in a two-dimensional interfacial layer or stratified/multi-layered is not known from our present study.

We then proceeded to evaluate the energetic aspects of this system. To this end, we divided the number of net-aligned Stern layer water molecules, $\mathcal{N}$, by their maximum value at the lowest ionic strength to obtain an order parameter, $s=\mathcal{N}/\mathcal{N}_{max}$. Relative to the reference state, $\mathcal{N}_{max}$, which is the most dilute case, we then express the Helmholtz free energy change, ΔF, as

$$\Delta F = -RT \ln(|s|) \quad (3)$$

Here, RT again is the thermal energy,[73] and here, we use the absolute value of s to avoid negative numbers in the ln. The free energy is the work associated with the Stern layer water rearrangement in response to the incoming ions. Fig. 2F shows that up to about 1 M ionic strength, the Helmholtz free energy is near zero or below thermal energy (2.5 kJ mol^{-1} at room temperature), indicating the interface is in a thermodynamically favorable state with well-aligned Stern layer water molecules. Once the ionic strength increases beyond 2 M, though, the Helmholtz free energy increases sharply, possibly indicating that the interface undergoes a Kirkwood transition out of a hydrated into a notably dehydrated state.

Concluding Remarks. In conclusion, this work employs a non-contact, all-optical method to estimate the surface coverages of cations, anions, and net-aligned water molecules on a solid (in

this case, fused silica) in contact with ionic solutions of sodium salts of common mono- and divalent anions up to 8 M ionic strength. At 8 M ionic strength of $NaClO_4$, the data are consistent with an interface that is comprised of half of a monolayer of ions ($\theta_{Na^+} + \theta_{ClO_4^-} \approx 5 \times 10^{14}$ cm^2) and half of a monolayer of water molecules ($\theta_{H_2O} \approx 4 \times 10^{14}$ cm^{-2}), the latter having flipped their dipolar orientation from "protons to the surface" at low ionic strength to "oxygens to the surface" at 8 M ionic strength. We caution that the interpretation of the experimental data presented here assumes that the second-order nonlinear susceptibility is primarily given by the interfacial water molecules and that the centrosymmetric ions (Na^+, Cl^-, ClO_4^-, SO_4^{2-}, HPO_4^{2-}) have only a minor, if any, contribution. In particular, our estimates of cation, anion, and net-aligned water densities will help elucidate the possible onset of contact ion pair formation as ionic strength increases. This insight will help predict the condition at which adding salt does not add more ions, thus helping us understand anomalous underscreening.

The results are consistent with an abrupt transition, perhaps of a Kirkwood type, from a hydrated to a dehydrated interface as the ionic strength exceeds 2 M, based on Helmholtz free energy arguments. We envision that the quantitative data may serve as experimental benchmarks for computational models and atomistic studies of the interface between solids and ionic solutions, including brines and water-in-salt mixtures. Such investigations could provide molecular-level structural information regarding possible stratification at the interface, contact vs. solvent-separated ion pair formation, and the slight overcharging that our data indicate via the sign flip in the total surface potential and the second-order non-linear susceptibility at ionic strength exceeding 5 M $NaClO_4$. The optical method presented here makes it, in principle, possible to carry out phase-resolved SHG imaging of water coverage and structure and ion surface coverages. Future studies are aimed at applying our method to quantify how the outcomes we describe in this present work, at room temperature, vary with increasing temperature. Our recent work shows increasing surface

deprotonation of silica with increasing temperature,[40] so probing this system under brine conditions would be of interest to areas in which hydrothermal conditions are relevant, such as crystal growth,[74] geothermal energy,[75] and mineral extraction,[76] as well as further investigation into a possible Kirkwood transition. Given our earlier report of decoupled Stern and diffuse layer dynamics under certain conditions of flow and pH[72] we also envision systematic variations of flow rate and acid base chemistry. Fundamental research into brines in contact with electrocatalysts is another area being pursued in this laboratory.

Supporting Information. Solution preparation details, SHG amplitude and face stability measurements, refractive index and decay length calculations, summary of total interfacial potential and interfacial structure as a function of concentration.

Acknowledgments. This work was supported by the US National Science Foundation (CHE-2153191, acknowledged for partial support of the oscillator and detection instrumentation, and CHE-2404203, acknowledged for support of NG). AA acknowledges support from a Saudi Aramco Graduate Fellowship.

Figure Captions

Figure 1. (**A**) SHG interference patterns as a function of quartz wafer position for $NaClO_4$ concentrations up to 8 M. (**B**) SHG amplitude normalized to the one obtained with deionized water at pH 6 and (**C**) SHG phase referenced to the point of zero charge (PZC) at pH 2.5 as a function of ionic strength for the salts indicated. Shading represents the standard deviation from 5 (*resp*. 8, 3, and 3) replicate measurements for NaCl (green circles) (*resp*. NaClO4 (yellow), Na_2SO_4 (red), and Na_2HPO_4 (black)) collected over multiple days using different silica substrates. All data for pH 5.8.

Figure 2. (**A**) Second-order nonlinear susceptibility and (**B**) number of net-aligned water molecules as a function of ionic strength for the salts indicated. Inset shows results for 1 to 8 M $NaClO_4$. (**C**) Total interfacial potential as a function of ionic strength for the salts indicated. (**D**) Interfacial ion coverages computed from the total interfacial potentials obtained as a function of ionic strength for the sodium salts indicated. Open and closed circles are for the anions and cations, respectively. (**E**) Ratio of net-aligned Stern layer water molecules and the total ion coverage as a function of ionic strength for the sodium salts indicated. Horizontal line indicates a 1:1 ratio. (**F**) Helmholtz free energy associated with net-aligned Stern layer water molecules as a function of water:ion pair ratio at the surface. The error bars represent the standard deviation from 5 (*resp*. 8, 3, and 3) replicate measurements for NaCl (green circles) (*resp*. NaClO4 (yellow), Na_2SO_4 (red), and Na_2HPO_4 (black)) collected over multiple days using different silica substrates. All data for pH 5.8.

Fig. 1

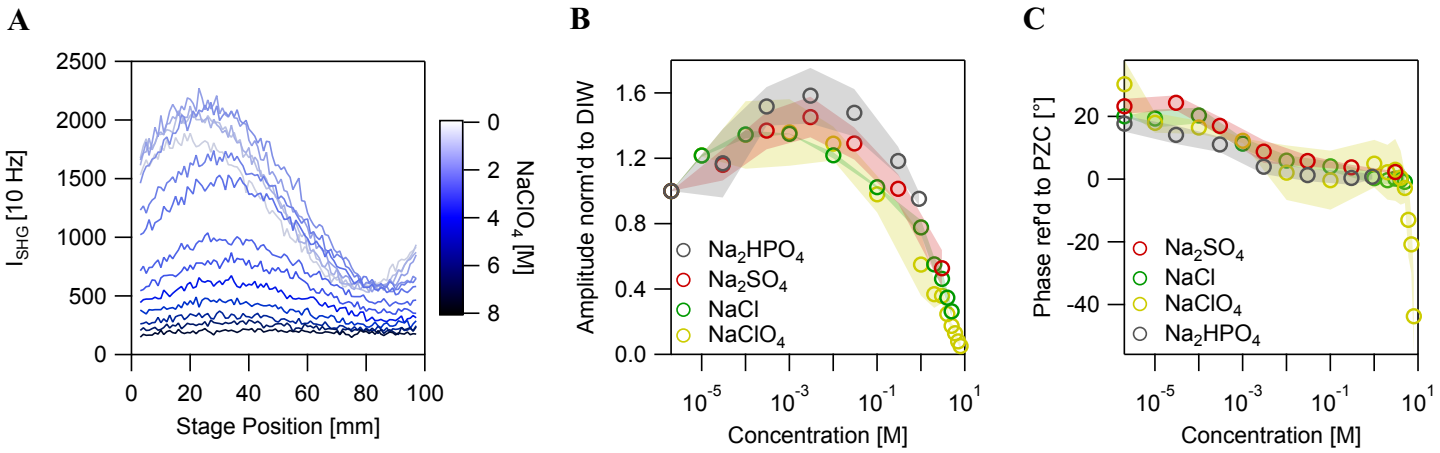
A
B
C
I_{SHG} [10 Hz]
Stage Position [mm]
$NaClO_4$ [M]
Amplitude norm'd to DIW
Concentration [M]
Phase ref'd to PZC [°]
Na_2HPO_4
Na_2SO_4
NaCl
$NaClO_4$

Fig. 2

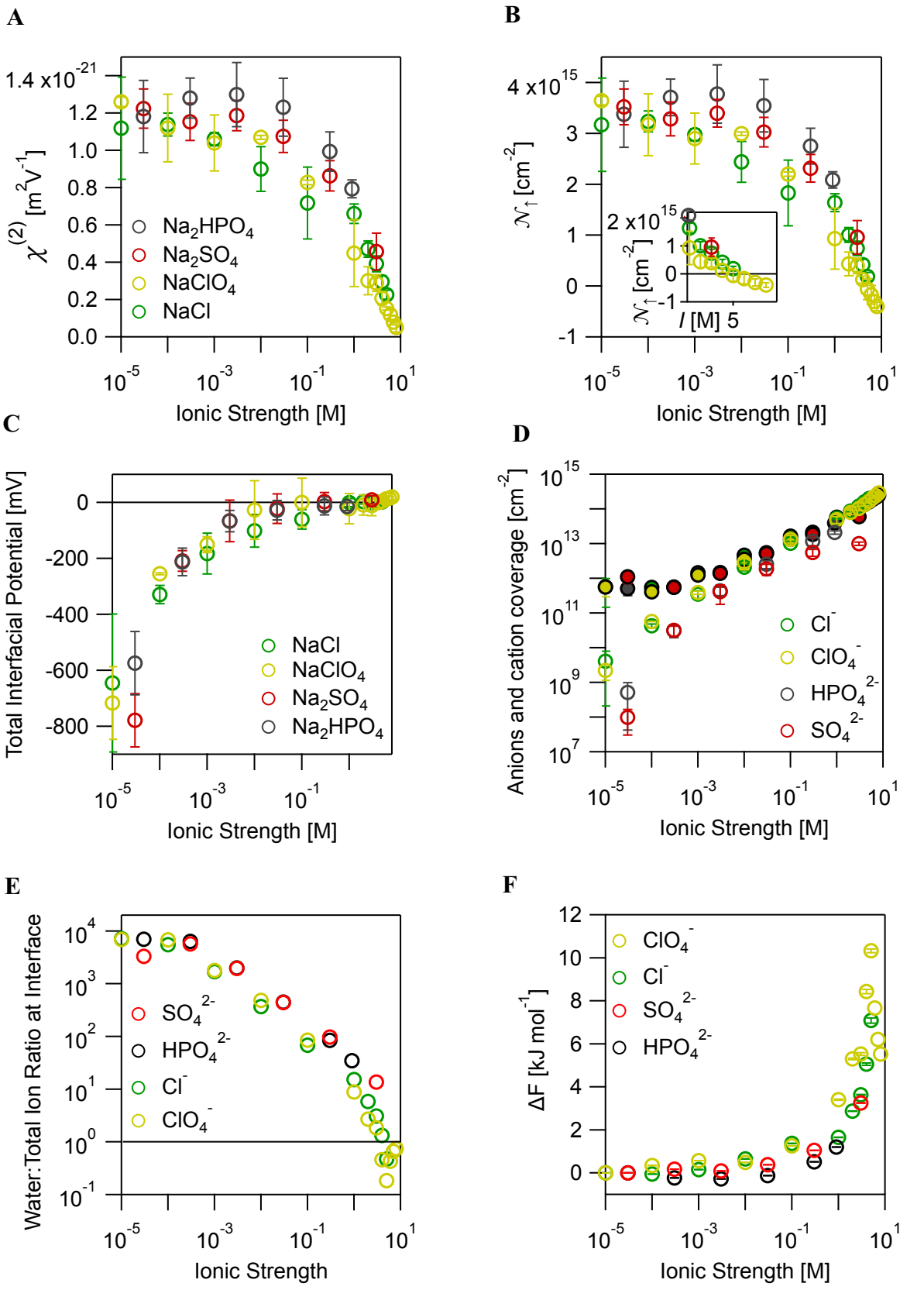
A
1.4 x10^-21
1.2
1.0
0.8
0.6
0.4
0.2
0.0
χ(2) [m2V-1]
Na2HPO4
Na2SO4
NaClO4
NaCl
10-5
10-3
10-1
101
Ionic Strength [M]
B
4 x10^15
3
2
1
0
-1
N↑ [cm-2]
2 x10^15
1
0
-1
N↑ [cm-2]
I [M] 5
10-5
10-3
10-1
101
Ionic Strength [M]
C
0
-200
-400
-600
-800
Total Interfacial Potential [mV]
NaCl
NaClO4
Na2SO4
Na2HPO4
10-5
10-3
10-1
Ionic Strength [M]
D
10^15
10^13
10^11
10^9
10^7
Anions and cation coverage [cm-2]
Cl-
ClO4-
HPO4 2-
SO4 2-
10-5
10-3
10-1
101
Ionic Strength [M]
E
10^4
10^3
10^2
10^1
10^0
10^-1
Water:Total Ion Ratio at Interface
SO4 2-
HPO4 2-
Cl-
ClO4-
10-5
10-3
10-1
101
Ionic Strength
F
12
10
8
6
4
2
0
ΔF [kJ mol-1]
ClO4-
Cl-
SO4 2-
HPO4 2-
10-5
10-3
10-1
101
Ionic Strength [M]

References

1. Hille, B., *Ion channels of excitable membranes, 3rd ed.* Oxford University Press: 2001.
2. Yousef, A. A.; Al-Saleh, S.; Al-Kaabi, A.; Al-Jawfi, M., Laboratory investigation of the impact of injection-water salinity and ionic content on oil recovery from carbonate reservoirs. *SPE Reservoir Evaluation & Engineering* **2011,** *14* (05), 578-593.
3. Prather, K. A.; Bertram, T. H.; Grassian, V. H.; Deane, G. B.; Stokes, M. D.; DeMott, P. J.; Aluwihare, L. I.; Palenik, B. P.; Azam, F.; Seinfeld, J. H.; Moffet, R. C.; Molina, M. J.; Cappa, C. D.; Geiger, F. M.; Roberts, G. C.; Russell, L. M.; Ault, A. P.; Baltrusaitis, J.; Collins, D. B.; Corrigan, C. E.; Cuadra-Rodriguez, L. A.; Ebben, C. J.; Forestieri, S. D.; Guasco, T. L.; Hersey, S. P.; Kim, M. J.; Lambert, W. F.; Modini, R. L.; Mui, W.; Pedler, B. E.; Ruppel, M. J.; Ryder, O. S.; Schoepp, N. G.; Sullivan, R. C.; Zhao, D., Bringing the ocean into the laboratory to probe the chemical complexity of sea spray aerosol. *Proc. Nat. Acad. Sci. USA* **2013,** *110* (19), 7550-7555.
4. Millero, F. J., *Chemical oceanography*. CRC press: 2005; Vol. 30.
5. Zhang, H.; Raciti, D.; Hall, A. S., Disordered interfacial H2O promotes electrochemical C–C coupling. *Nature Chemistry* **2025,** *17* (8), 1161-1168.
6. Yamada, Y.; Yamada, A., Superconcentrated electrolytes for lithium batteries. *Journal of the Electrochemical Society* **2015,** *162* (14), A2406.
7. Suo, L.; Borodin, O.; Gao, T.; Olguin, M.; Ho, J.; Fan, X.; Luo, C.; Wang, C.; Xu, K., "Water-in-salt" electrolyte enables high-voltage aqueous lithium-ion chemistries. *Science* **2015,** *350* (6263), 938-943.
8. Conway, B. E., *Electrochemical supercapacitors: scientific fundamentals and technological applications*. Springer Science & Business Media: 2013.
9. Fröhlich, E., The role of surface charge in cellular uptake and cytotoxicity of medical nanoparticles. *International journal of nanomedicine* **2012**, 5577-5591.
10. Bachu, S., CO2 storage in geological media: Role, means, status and barriers to deployment. *Progress in Energy and Combustion Science* **2008,** *34* (2), 254-273.
11. Bañuelos, J. L.; Borguet, E.; Brown Jr, G. E.; Cygan, R. T.; DeYoreo, J. D.; Dove, P. M.; Gaigeot, M.-P.; Geiger, F. M.; Gibbs, J. M.; Grassian, V. H.; Ilgen, A. G.; Jun, Y.-S.; Kabengi, N.; Katz, L.; Kubicki, J. D.; Lützenkirchen, J.; Putnis, C. V.; Remsing, R. C.; Rosso, K. M.; Rother, G.; Sulpizi, M.; Villalobos, M.; Zhang, H., Oxide–and Silicate–Water Interfaces and Their Roles in Technology and the Environment. *Chemical Reviews* **2023,** *123*, 6413-6544.
12. Gonella, G.; Backus, E. H.; Nagata, Y.; Bonthuis, D. J.; Loche, P.; Schlaich, A.; Netz, R. R.; Kuehnle, A.; McCrum, I. T.; Koper, M. T. M.; Wolf, M.; Winter, B.; Meijer, G.; Campen, R. K.; Bonn, M., Water at Charged Interfaces. *Nat. Rev. Chem.* **2021,** *5*, 466-85.
13. Elliott, G. R.; Gregory, K. P.; Robertson, H.; Craig, V. S.; Webber, G. B.; Wanless, E. J.; Page, A. J., The known-unknowns of anomalous underscreening in concentrated electrolytes. *Chemical Physics Letters* **2024**, 843, 141190.
14. Reinertsen, R. J.; Kewalramani, S.; Jiménez-Ángeles, F.; Weigand, S. J.; Bedzyk, M. J.; Olvera de la Cruz, M., Reexpansion of charged nanoparticle assemblies in concentrated electrolytes. *Proceedings of the National Academy of Sciences* **2024,** *121* (6), e2316537121.
15. Fung, Y. C.; Perkin, S., Structure and anomalous underscreening in ethylammonium nitrate solutions confined between two mica surfaces. *Faraday Discussions* **2023,** *246*, 370-386.
16. Smith, A. M. L., A. A.; Perkin, S. , The Electrostatic Screening Length in Concentrated Electrolytes increasing with Concentration. *Journal of Physical Chemistry B* **2019,** *123* (7), 1733-1740.

17. Smith, A. M.; Maroni, P.; Trefalt, G.; Borkovec, M., Unexpectedly large decay lengths of double-layer forces in solutions of symmetric, multivalent electrolytes. *The Journal of Physical Chemistry B* **2019,** *123* (7), 1733-1740.
18. Gebbie, M. A., Smith, A. M., Dobbs, H. A., Lee, A. A., Warr, G. G., Banquy, X., Valtiner, M., Rutland, M. W., Israelachvili, J. N., Perkin, S., Atkin, R. Long range electrostatic forces in ionic liquids. *Chemical Communications* **2017,** 53 (7), 1214-24.
19. Goodwin, Z. A.; Kornyshev, A. A., Underscreening, overscreening and double-layer capacitance. *Electrochemistry Communications* **2017,** *82*, 129-133.
20. Baimpos, T.; Shrestha, B. R.; Raman, S.; Valtiner, M., Effect of interfacial ion structuring on range and magnitude of electric double layer, hydration, and adhesive interactions between mica surfaces in 0.05–3 M Li+ and Cs+ electrolyte solutions. *Langmuir* **2014,** *30* (15), 4322-4332.
21. Rondepierre, F.; Brevet, P.-F.; Duboisset, J., Asymptotic Underscreening in Concentrated Electrolytes Measured by Optical Second Harmonic Scattering of Water. *J. Phys. Chem. Lett.* **2025,** *16*, 2690-2694.
22. Lewis, N. H. C.; Dereka, B.; Zhang, Y.; Maginn, E. J.; Tokmakoff, A., From Networked to Isolated: Observing Water Hydrogen Bonds in Concentrated Electrolytes with Two-Dimensional Infrared Spectroscopy. *J. Phys. Chem. B* **2022,** *126*, 5305-19.
23. Ribar, D.; Woodward, C. E.; Forsman, J., Solvent-induced ion clusters generate long-ranged double-layer forces at high ionic strengths. *Soft Matter* **2025,** *21*, 5562-72.
24. Berlinger, S. A.; Kuepers, V.; Dudenas, P. J.; Schinski, D.; Flagg, L.; Lamberty, Z. D.; McCloskey, B. D.; Winter, M.; Frechette, J., Cation valency in water-in-salt electrolytes alters the short- and long-range structure of the electrical double layer. *Proc. Nat. Acad. Sci. USA* **2024,** *121*, e2404669121.
25. Wang, S.; Tao, H.; Yang, J.; Cheng, J.; Lian, C., Structure and Screening in Confined Electrolytes: The Role of Ion Association. *J. Phys. Chem. Lett.* **2024,** *15*, 7147-53.
26. Kant, R.; Goswami, N., Semimicroscopic Theory for Underscreening-Induced Anomalous Migration–Diffusion Coupling. *J. Phys. Chem. C* **2021,** *125*, 13677-87.
27. Haagh, M. E.; Siretanu, I.; Mugele, F., Salinity-Dependent Contact Angle Alteration in Oil/Brine/Silicate Systems: the Critical Role of Divalent Cations. *Langmuir* **2017,** *33*, 3349-57.
28. Tsuyoshi, J.; Bao, Y.; Ichii, T.; Utsunomiya, T.; Sugimura, H., Effect of anion on water-in-salt/solid interfacial structures investigated by atomic force microscopy. *Jap. J. Appl. Phys.* **2022,** *61*, SL1003.
29. Smith, M. A. M., P; Trefalt, G.; Borokovec, M. , Unexpectedly large decay lengths of double-layer forces in solutions of symmetric, multivalent electrolytes. *Journal of Physical Chemistry B* **2019,** *123* (7), 1733-1740.
30. Baimpos, T. S., B. R.; Raman, S.; Valtiner, M. , Effect of Interfacial Ion Structuring on range and Magnitude of Electrical Double Layer, Hydration, and Adhesive Interactions between Mica Surfaces in 0.05 - 3M Li+ and Cs+ Electrolyte Solutions. *Langmuir* **2014,** *30* (15), 4322-4332.
31. Espinosa-Marzal, R. M.; Drobek, T.; Balmer, T.; Heuberger, M. P., Hydrated-ion ordering in electrical double layers. *Physical Chemistry Chemical Physics* **2012,** *14* (17), 6085-6093.
32. Perez-Martinez, C. S.; Smith, A. M.; Perkin, S., Underscreening in concentrated electrolytes. *Faraday Discussions* **2017,** *199*, 239-259.
33. Kirkwood, J. G.; Poirier, J. C., The statistical mechanical basis of the Debye–hüekel theory of strong electrolytes. *The Journal of Physical Chemistry* **1954,** *58* (8), 591-596.
34. Dinpajooh, M.; Biasin, E.; Nienhuis, E. T.; Mergelsberg, S. T.; Benmore, C. J.; Schenter, G. K.; Fulton, J. L.; Kathmann, S. M.; Mundy, C. J., Detecting underscreening and generalized

Kirkwood transitions in aqueous electrolytes. *The Journal of Chemical Physics* **2024,** *161* (15) 151102.
35. Adar, R. M.; Safran, S. A.; Diamant, H.; Andelman, D., Screening length for finite-size ions in concentrated electrolytes. *Physical Review E* **2019,** *100* (4), 042615.
36. Kjellander, R., Decay behavior of screened electrostatic surface forces in ionic liquids: the vital role of non-local electrostatics. *Physical Chemistry Chemical Physics* **2016,** *18* (28), 18985-19000.
37. Lee, S. S.; Koishi, A.; Bourg, I. C.; Fenter, P., Ion correlations drive charge overscreening and heterogeneous nucleation at solid–aqueous electrolyte interfaces. *Proceedings of the National Academy of Sciences* **2021,** *118* (32), e2105154118.
38. Jena, K. C.; Covert, P. A.; Hore, D. K., The effect of salt on the water structure at a charged solid surface: differentiating second-and third-order nonlinear contributions. *The Journal of Physical Chemistry Letters* **2011,** *2* (9), 1056-1061.
39. Olson, A. L.; Alghamdi, A. O.; Geiger, F. M., NaCl, MgCl2, and AlCl3 surface coverages on fused silica and adsorption free energies at pH 4 from nonlinear optics. *The journal of physical chemistry A* **2024,** *128* (11), 2162-2168.
40. Alghamdi, A. O.; Gonzalez, N. M.; Geiger, F. M., Temperature Dependence of Proton Coverage and the Total Potential at Fused Silica: Water Interfaces from Phase-Resolved Nonlinear Optics. *Journal of the American Chemical Society* **2025,** *147* (17), 14308-14315.
41. Speelman, R.; Marker, E. J.; Geiger, F. M., Quantifying Stern layer water alignment before and during the oxygen evolution reaction. *Science Advances* **2025,** *11* (10), eado8536.
42. Hamer, W. J.; Qu, Y.-C., Osmotic Coefficients and Mean Activity Coefficients of Uni-univalent Electrolytes in Water at 25°C. *J. Phys. Chem. Ref. Data* **1972,** *1*, 1047-1100.
43. Ma, E.; Ohno, P. E.; Kim, K.; Liu, Y.; Lozier, E. H.; Miller III, T. F.; Wang, H.-f.; Geiger, F. M., A New Imaginary Term in the 2nd Order Nonlinear Susceptibility from Charged Interfaces. *J. Phys. Chem. Lett.* **2021,** *12* (24), 5649-59.
44. Ohno, P. E.; Saslow, S. A.; Wang, H.; Geiger, F. M.; Eisenthal, K. B., Phase referenced nonlinear spectroscopy of the alpha-quartz/water interface. *Nat. Commun.* **2016,** *7*, 13587.
45. We first reported this effect in SHG intensity measurements published in Achtyl, J. L.; Vlassiouk, I. V.; Fulvio, P. F.; Mahurin, S. M.; Dai, S.; Geiger, F. M., Free Energy Relationships in the Electrical Double Layer over Single-Layer Graphene. J. Am. Chem. Soc. 2013, 135, 979-981.
46. Olson, A. L.; Alghamdi, A. O.; Geiger, F. M., NaCl, MgCl2, and AlCl3 Surface Coverages on Fused Silica and Adsorption Free Energies at pH 4 From Nonlinear Optics. *J. Phys. Chem. A* **2024,** *128*, 2162-8.
47. Chang, H.; Lozier, E. H.; Ma, E.; Geiger, F. M., Quantification of Stern Layer Water Molecules, Total Potentials, and Energy Densities at Fused Silica:Water Interfaces for Adsorbed Alkali Chlorides, CTAB, PFOA, and PFAS. *J. Phys. Chem. A* **2023,** *127*, 8404-14.
48. Ohno, P. E.; Wang, H.-f.; Geiger, F. M., Second-order spectral lineshapes from charged interfaces. *Nature Comm.* **2017,** *8* (1), 1032.
49. Reddy, S. K.; Thiraus, R.; Rudd, B. A. W.; Lin, L.; Adel, T.; Joutsuka, T.; Geiger, F. M.; Allen, H. C.; Morita, A.; Paesani, F., Bulk Contributions Modulate the Sum-Frequency Generation Spectra of Water on Model Sea-Spray Aerosols. *Chem.* **2018,** *4*, 1629-1644.
50. Rehl, B.; Ma, E.; Parshotam, S.; DeWalt-Kerian, E. L.; Liu, T.; Geiger, F. M.; Gibbs, J. M., Water structure in the electrical double layer and the contributions to the total interfacial potential at different surface charge densities. *Journal of the American Chemical Society* **2022,** *144* (36), 16338-16349.

51. Lütgebaucks, C.; Gonella, G.; Roke, S., Optical label-free and model-free probe of the surface potential of nanoscale and microscopic objects in aqueous solution. *Physical Review B* **2016,** *94* (19), 195410.
52. Bischoff, M.; Biriukov, D.; Předota, M.; Roke, S.; Marchioro, A., Surface potential and interfacial water order at the amorphous TiO2 nanoparticle/aqueous interface. *The Journal of Physical Chemistry C* **2020,** *124* (20), 10961-10974.
53. Wei, F.; Urashima, S.-h.; Nihonyanagi, S.; Tahara, T., Elucidation of the pH-dependent electric double layer structure at the silica/water interface using heterodyne-detected vibrational sum frequency generation spectroscopy. *Journal of the American Chemical Society* **2023,** *145* (16), 8833-8846.
54. Nihonyanagi, S.; Ishiyama, T.; Lee, T.-k.; Yamaguchi, S.; Bonn, M.; Morita, A.; Tahara, T., Unified molecular view of the air/water interface based on experimental and theoretical χ (2) spectra of an isotopically diluted water surface. *Journal of the American Chemical Society* **2011,** *133* (42), 16875-16880.
55. Uddin, M. M.; Azam, M. S.; Hore, D. K., Variable-angle surface spectroscopy reveals the water structure in the stern layer at charged aqueous interfaces. *Journal of the American Chemical Society* **2024,** *146* (17), 11756-11763.
56. Darlington, A. M.; Jarisz, T. A.; DeWalt-Kerian, E. L.; Roy, S.; Kim, S.; Azam, M. S.; Hore, D. K.; Gibbs, J. M., Separating the pH-dependent behavior of water in the stern and diffuse layers with varying salt concentration. *The Journal of Physical Chemistry C* **2017,** *121* (37), 20229-20241.
57. Speelman, R.; Marker, E. J.; Boamah, M. D.; Kupferberg, J.; Bye, J. Z.; Engelhard, M.; Zhao, Y.; Martinson, A. B. F.; Rosso, K. M.; Geiger, F. M., Water flipping and the oxygen evolution reaction on Fe2O3 nanolayers. *Nature Comm.* **2025,** *16* (1), 3585.
58. Levine, B. F.; Bethea, C. G., Effects on hyperpolarizabilities of molecular interactions in associating liquid mixtures. *Journal of Chemical Physics* **1976,** *65* (6), 2429-38.
59. Gubskaya, A. V.; Kusalik, P. G., The multipole polarizabilities and hyperpolarizabilities of the water molecule in liquid state: an ab initio study. *Mol. Phys.* **2001,** *99*, 1107-20.
60. Dewan, S.; Carnevale, V.; Bankura, A.; Eftekhari-Bafrooei, A.; Fiorin, G.; Klein, M. L.; Borguet, E., Structure of Water at Charged Interfaces: A Molecular Dynamics Study. *Langmuir* **2014,** *30*, 8056-65.
61. Wang, R. Y.; Klein, M. L.; Carnevale, V.; Borguet, E., Investigations of water/oxide interfaces by molecular dynamics simulations. *Wiley Interdisciplinary Reviews-Computational Molecular Science* **2021,** *11* (6), 26.
62. Darlington, A. M.; Jarisz, T. A.; DeWalt-Kerian, E. L.; Roy, S.; Kim, S. H.; Azam, M. S.; Hore, D. K.; Gibbs, J. M., Separating the pH-Dependent Behavior of Water in the Stern and Diffuse Layers with Varying Salt Concentration. *J. Phys. Chem. C* **2017,** *121*, 20229-20241.
63. Covert, P. A.; Jena, K. C.; Hore, D. K., Throwing Salt into the Mix: Altering Interfacial Water Structure by Electrolyte Addition. *J. Phys. Chem. Lett.* **2014,** *5*, 143-148.
64. Israelachvili, J. N., *Intermolecular and surface forces*. Academic press: 2011.
65. Peng, M. S.; Duignan, T. T.; Zhao, X. S.; Nguyen, A. V., Surface Potential Explained: A Surfactant Adsorption Model Incorporating Realistic Layer Thickness. *J. Phys. Chem. B* **2020,** *124*, 3195-205.
66. EL Alaoui, S. M. A.; Ghallali, L.; EL Guendouzi, M.; Benbiyi, A., Solubility and Thermodynamic Properties of Dipotassium or Disodium Hydrogenphosphates in Aqueous Solutions at Various Temperatures. *J. Sol. Chem.* **2022,** *51*, 802-15.

67. EL Guendouzi, M.; Mounir, A.; Dinane, A., Water activity, osmotic and activity coe9cients of aqueous solutions of Li2SO4, Na2SO4, K2SO4, NH42SO4, MgSO4, MnSO4, NiSO4, CuSO4, and ZnSO4 at T= 298:15 K. *J. Chem. Therm.* **2003,** *35*, 209-20.
68. Stokes, J. M., The osmotic and activity coefficients of sodium and potassium dihydrogen phosphate at 25 deg C. *Farad. Disc.* **1945,** *41*, 685-8.
69. We note that IUPAC recommends against the use of single ion activities because they cannot be measured independently.
70. Rockwood, A. L., Meaning and Measurability of Single-Ion Activities, the Thermodynamic Foundations of pH, and the Gibbs Free Energy for the Transfer of Ions between Dissimilar Materials. *ChemPhysChem* **2015,** *16*, 1978-91.
71. Uzzo, A.; Daghetti, A.; Trasatti, S., Single ion activity coefficients based on the electrical double-layer model. Na2SO4 aqueous solutions. *Electrochim. Acta* **1983,** *28*, 1539-44.
72. Ma, E.; Kim, J.; Chang, H.; Ohno, P. E.; Jodts, R. J.; Miller III, T. F.; Geiger, F. M., Stern and Diffuse Layer Interactions during Ionic Strength Cycling. *J. Phys. Chem. C* **2021,** *125*, 18002-14.
73. Dill, K. A.; Bromberg, S., *Molecular Driving Forces: Statistical Thermodynamics in Biology, Chemistry, Physics, and Nanoscience*. 2 ed.; Taylor & Francis: New York, NY, 2011.
74. Demazeau, G.; Largeteau, A., Hydrothermal/Solvothermal Crystal Growth: an Old but Adaptable Process. *Z. Anorg. Allg. Chemie* **2014,** *641*, 159-63.
75. Sharmin, T.; Khan, N. R.; Akram, M. S.; Ehsan, M. M., A State-of-the-Art Review on Geothermal Energy Extraction, Utilization, and Improvement Strategies: Conventional, Hybridized, and Enhanced Geothermal Systems. *Int. J. Thermofluids* **2023,** *8*, 1000323.
76. Ryu, J.; Kim, S.; Hong, H. J.; Hong, J.; Kim, M.; Ryu, T.; Park, I. S.; Chung, K. S.; Jang, J. S.; Kim, B. G., Strontium ion (Sr^{2+}) separation from seawater by hydrothermally structured titanate nanotubes: Removal vs. recover. **2016,** *304*, 503-510.

TOC Graphic